JOURNAL OF MATERIALS SCIENCE **38** (2003) 877–884

# Time-dependent micromechanical behavior in graphite/epoxy composites under constant load at elevated temperatures

C. H. ZHOU
*Materials Science and Engineering, Rensselaer Polytechnic Institute, Troy, NY12180, USA*

I. J. BEYERLEIN
*Los Alamos National Laboratory, Los Alamos, MS G755, NM 87545, USA*

L. S. SCHADLER*
*Materials Science and Engineering, Rensselaer Polytechnic Institute, Troy, NY12180, USA*
*E-mail: schadl@rpi.edu*

Time dependent deformation at the individual fiber level was investigated in graphite fiber/epoxy composites at elevated temperatures using micro Raman spectroscopy (MRS) and a time dependent shear-lag based single fiber composite model (SFM). The modeling parameters were obtained from the creep response of the unfilled epoxy at several stress levels and at temperatures up to 80°C. An effective fiber spacing was used in the model predictions to account for the radial decay of the interfacial shear stress from the fiber surface. Good agreement was observed between the model predictions and MRS data when the temperature dependence of $\tau_p$ (the shear stress in the matrix yielded zone) and $\gamma_c$ (the critical shear strain for the onset of inelasticity) were taken into account. Overall, the inelastic length growing from the fiber fractures increases with temperature and time. This leads to a wider stress concentration profile in the neighboring intact fibers, which increases the chance of failure in the intact fibers and facilitates the creep-rupture process of the composite. 

## 1. Introduction

It is generally believed that the time to creep-rupture of polymer matrix composites decreases at elevated temperatures. Gramoll *et al.* [1] investigated the creep of a Kevlar/epoxy laminate at elevated temperatures from 30°C to 105°C. They noticed that failure of the composite samples occurred at higher temperature and in a time-dependent fashion. This observation suggests that the failure process was accelerated along with viscoelastic behavior at high temperatures. Greenwood's work [2] on carbon/epoxy composites also showed that a high temperature environment decreased the time to fracture.

Creep-rupture results from the time dependent nucleation and growth of localized damage, such as fiber breaks, interfacial debonding, and voids, which are undetectable on the macroscopic scale. A full understanding of the micromechanical behavior is essential in order to predict creep-rupture of polymer composites.

One method for measuring the micromechanical response of graphite fiber/transparent polymer matrix composites is micro-Raman spectroscopy (MRS). MRS can be used to measure the distribution of axial strain along a graphite fiber with a spatial resolution of 1–2 $\mu$m. Galiotis *et al.* [3] used Raman spectroscopy to measure the strain in a polydiacetylene fiber in an epoxy resin and studied the strength of the bonding between the polymer matrix and the fiber. Miyake *et al.* [4] investigated the stress relaxation behavior around a break in single fiber model composites. It was observed that the stress profile in the broken fiber did not change significantly after 1000 hours, while the matrix tensile stress in the fiber direction relaxed to about a quarter of its initial value in about 200 hours. Thomson and Pyrz [5, 6] investigated the load transfer as a function of time in carbon/polypropylene model composites. Their MRS measurements were compared with their non-linear creep model. Only qualitative agreement was found.

In previous work, we investigated the strain/stress evolutions in individual fibers due to a constant load at room temperature [7, 8]. MRS was used for *in situ* measurement of the fiber strain in the composite and shear lag-based micromechanical models were developed to predict the matrix shear dominated strain/stress evolution in the composite driven by fiber breaks. Both the single fiber and multifiber models we developed assumed appropriately that the matrix is viscoelastic [7, 9, 10]. We demonstrated that these models can use

*Author to whom all correspondence should be addressed.

parameters determined from the creep behavior of the bulk matrix to predict the *in situ* local matrix creep behavior around a fiber break and to predict time dependent stress transfer. Also in these PMCs, interfacial slip or matrix inelasticity grew from the fractures with time, exhibiting a significant effect on stress transfer [7, 8]. Simple extensions of our viscoelastic composite models to account for local damage development enabled insightful interpretation of the MRS data [8]. All analyses and tests were conducted at room temperature. Elevated temperatures, however, will certainly alter both damage development and time dependent stress transfer.

Fig. 1 illustrates a typical axial strain distribution and corresponding interfacial shear stress as a function of distance from the fiber break in a graphite fiber/epoxy matrix system measured using MRS. The strain in the fiber increases from zero at the end, to the applied strain via a shear stress at the interface. When the shear stress is less than the debonding stress and the yield stress of the matrix, the load transfer is elastic and the axial strain along the broken fiber builds up rapidly from the fiber end. If the applied strain is high enough, regions of matrix yielding and interfacial debonding near the fiber break are very likely. In these "inelastic" interfacial regions, the fiber axial strain builds up roughly linearly (See Fig. 1), indicating that the interfacial shear stress is approximately constant. This value is denoted as $\tau_c$ and is usually related to the matrix shear strength or by frictional sliding resistance in the debonded region. In our work, $\tau_p$ is used for the matrix shear stress in the 'plastic' zone and $\tau_d$ for the interfacial shear stress in the interfacial sliding zone. In the viscoelastic region away from the break end, the interface is intact and the fiber axial strain increases non-linearly until it reaches the applied axial strain $\varepsilon^*$. Correspondingly the interfacial shear stress gradually decreases from a peak value, $\tau_{max}$, to zero.

From these MRS profiles, one can characterize important length scales of load transfer. The first is the distance between the fiber break and the $\tau_{max}$, which is defined as the inelastic length, $l(t)$. The second is the load recovery length, $L_r$, which is the distance between $\tau_{max}$ and the point where $\tau$ decreases to about zero. A 'cut-off' criterion is usually used to determine $L_r$. For example, in the previous work [7], we used the ratio

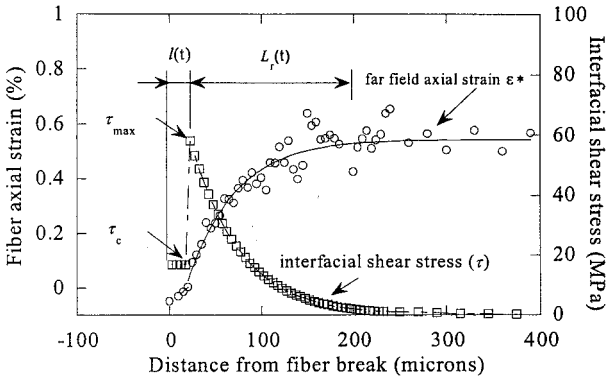


*Figure 1* Typical fiber axial strain and interfacial shear stress distribution around a break in a model multi-fiber composite.

$\tau/\tau_{max} = 5\%$. A more common criterion is based on a cut-off fiber strain, which is a certain fraction of the far field strain. It was shown [8] that the time evolution of $L_r$ is independent of the length and type of inelastic zone when defined using a cut-off shear stress unlike when using a cut-off fiber strain.

As the matrix relaxes locally around the fiber break, the fiber strain and the shear stress profiles (and hence $l_{in}$ and $L_r$) shown in Fig. 1 will change accordingly. Such changes in stress distribution will influence the time progression of new fiber breaks and ultimately creep rupture. Furthermore the rate of matrix relaxation [11, 12] and hence stress transfer will also vary with testing temperature, resulting in a significant impact on time to creep rupture. Testing at elevated temperature is particularly important, not only for material performance at anticipated service temperatures but also for accelerated lifetime testing of polymers and polymer composites. It is still unclear, however, how to extrapolate, for instance, the short-term data at high temperatures to the long-term creep rupture at room temperature. Before such time scaling laws can be developed, the influence of matrix relaxation around fractures in multifiber composites as a function of temp and composite fiber volume fraction need to be characterized and modeled.

## 2. Modeling approach

Predictions from an inelastic-viscoelastic single fiber composite model (SFM) developed in [8] were compared with MRS data. The incorporation of inelasticity has greatly expanded the predictive capability and applicability from that of the original viscoelastic SFM, first presented in [7]. Here is a brief description of the axisymmetric SFM based on shear-lag analysis. Details of the derivations can be found in [8].

As illustrated in Fig. 2a, the single fiber model with radius $w$ or $w'$ is intended to represent a periodic unit cell in a 2 dimensional fiber arrangement. Fig. 2b illustrates a different view of the axisymmetric SFM geometry, where a single fracture is located at $x = 0$ and a steady uniform load is applied far field. The time-independent elastic fibers sustain the axial stress (or strain) applied to the composite. The shear-lag based model assumes that the matrix deforms or creeps only in shear, and prior to the onset of inelastic behavior, the matrix is linearly viscoelastic with the creep shear compliance $J(t)$ following either a complete power law function or an incomplete power law function, as shown below.

$$J(\mathcal{T}) = J_1[1 + (\mathcal{T}/\mathcal{T}_C)^{\alpha}] \quad \{\text{complete}\} \qquad (1)$$

$$J(\mathcal{T}) = J_e(\mathcal{T}/\mathcal{T}_C)^{\alpha} \quad \{\text{incomplete}\} \qquad (2)$$

Based on these assumptions, the model stresses and displacements will depend only on $x$, the fiber axial coordinate, and the normalized time $t$, $t = \mathcal{T}/\mathcal{T}_C$.

The shear stress-displacement behavior of the matrix or interface close to the fiber is assumed to follow the elastic-inelastic constitutive law in Fig. 3. The inelastic interfacial shear stress $\tau_c(t)$ is a function of time, but independent of space and can represent the shear

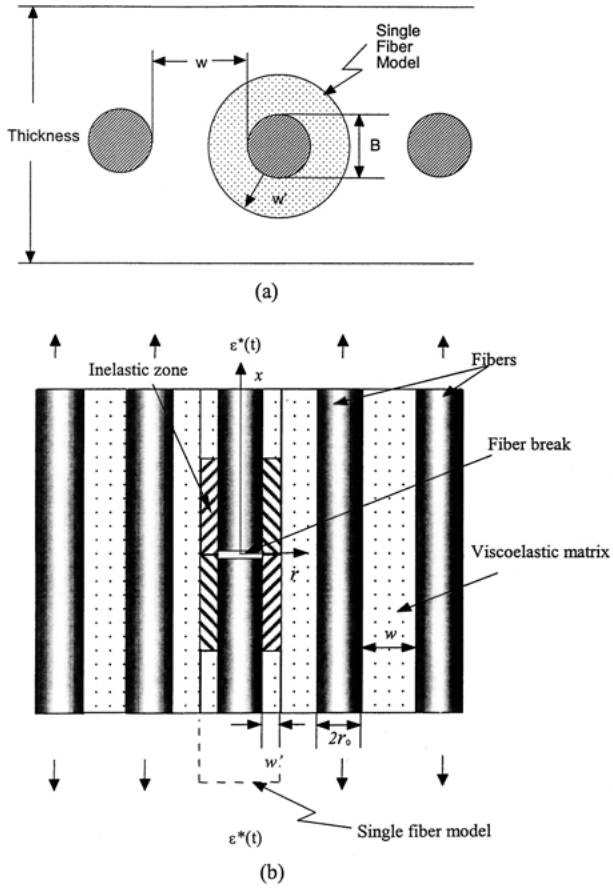


*Figure 2* Geometry of the 2-D fiber array used in the single fiber model (SFM) (a) cross-section; (b) longitude section.

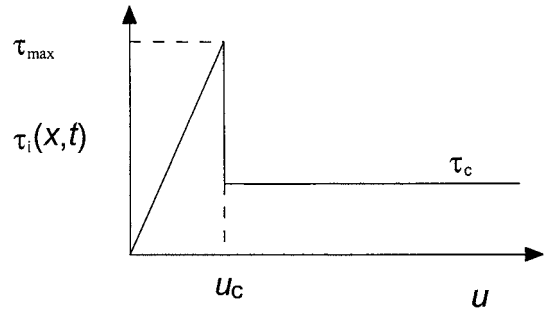


*Figure 3* Shear stress-displacement behavior of the matrix/fiber interface.

resistance by either matrix shear yielding or interfacial sliding friction of a failed interface. A more complicated law, namely the elastic-plastic-slip law, was considered as well in [8]. The onset of an inelastic zone of length $l(t)$ from the break site at $x = 0$ at time $t$ is considered to occur when the bonded, elastic interface reaches either a critical shear displacement denoted $u_c$ or shear strain $\gamma_c$ at $x = 0$, which will be determined by comparison with MRS data. In the following equations, $u_c$ is used, though it can be converted to $\gamma_c$ using $u_c = \gamma_c w$.

The fiber strain in the inelastic zone [8] is

$$\varepsilon(x,t) = k_l \tau_c(t) x + \varepsilon_r(t), \quad 0 < x < l(t) \qquad (3)$$

where $k_l = \frac{B}{AE}$, $A = \pi r_0^2$, $B = 2\pi r_0 = \pi d$, $E$ is the Young's modulus of the fiber, and $r_0$ and $d$ are the fiber radius and diameter. Note that the SFM considers the residual fiber strain $\varepsilon_r(t)$ at the break, $x = 0$, which can possibly change with time.

The fiber strain is obtained for the viscoelastic zone,

$$\varepsilon(x,t) \approx -u_c K(t) \exp[-K(t)(x - l(t))] + \varepsilon^*(t) \qquad l(t) \le x < \infty \qquad (4)$$

where

$$K(t) = k_0 \sqrt{\mu(t)}|_{s=\exp(-\gamma_s)/t}, \quad k_0^2 = \frac{B}{EAwJ_1},$$

$\gamma_s$ is Euler's constant ~0.5772. Subsequently, the interfacial shear stress $\tau_i(x,t)$, within the viscoelastic zone is

$$\tau_i(x,t) = \frac{EA}{B} K(t)[(\varepsilon^*(t) - \varepsilon_r(t)) - k_l \tau_c(t) l(t)] \times \exp[-K(t)(x - l(t)], \quad l(t) \le x < \infty \qquad (5)$$

Values for the far field strain $\varepsilon^*(t)$ and the residual strain $\varepsilon_r(t)$ used in the model are those measured in the fiber at each measurement time.

Equating Equations 3 and 4 for the fiber strain at $x = l(t)$ to enforce continuity in fiber strain at $x = l(t)$ gives an expression for $l(t)$

$$l(t) = \frac{((\varepsilon^*(t) - \varepsilon_r(t)) - u_c K(t))}{k_l \tau_c(t)}, \quad l(t) \ge 0 \qquad (6)$$

In the above equations, $\mu(t)$ depends on the model used for the matrix creep compliance, as shown below.

$$\mu_C(t) = \frac{1}{1 + k_2 t^\alpha} \quad \{\text{Complete law, Equation 1}\} \qquad (7a)$$

$$\mu_e(t) = \frac{1}{k_2 t^\alpha} \quad \{\text{Incomplete law, Equation 2}\} \qquad (7b)$$

where $k_2 = \Gamma(1+\alpha)\exp(\alpha\gamma_s)$. Previous work [10] has shown that the incomplete power law gives almost indentical strain/stress predictions as the complete power law function. We demonstrate in [8] that these two functions lead to different predictions when the time is significantly shorter than the characteristic time associated with Equation 2. Because the time required to take the first MRS measurements is longer than the characteristic time, only predictions using the complete power law are presented in this work.

Our MRS work [7] indicates that there is little change in $\tau_c(t)$ as time progresses. Therefore, the creep of the matrix within the inelastic length $l(t)$ is ignored and $\tau_c$ is assumed to be constant with the value depending on the interfacial condition.

In the above derivations, the matrix shear stress $\tau(x,t)$ and the shear strain $\gamma(x,t)$ are assumed to be constant over the fiber spacing $w$, independent of the radial distance from the center of the fiber. However, for low fiber volume fractions where $w \gg r_0$, significant shear deformation usually occurs close to the interface and decreases radially away from the fiber surface.

Accordingly, the assumption of a constant shear stress between the fiber surfaces is not valid when $w$ is relatively large. An effective fiber spacing $w'$ is used in place of the measured $w$ in the model. The expression for $w'$ is shown in Equation 8, while the details of the derivations can be found in [8].

$$w' = r_0 \ln\left(\frac{r_0 + w}{r_0}\right), \quad w > r_0 \tag{8a}$$

$$w' = w, \quad w \le r_0 \tag{8b}$$

## 3. Experimental procedure

### 3.1. Creep tests of the composite

Fig. 4 shows the geometry of the model fiber composite specimen for the MRS monitored creep tests. The matrix material is an epoxy (Epon828 + Epi-Cure3234 curing agent at 1:0.129 ratio) and the graphite fiber is a high modulus Toray M40B. The preparation of the composite specimens was described in detail in [7]. All specimens were cured at room temperature for 12 hrs and post-cured at 100°C for 2 hrs. Table I lists some details for the four specimens, such as the fiber spacing, the fiber strain and the observed debonding near the fiber break. It should be noted that in specimens H1 and H7, there were two fiber arrays with very different fiber spacing. Since the two fiber arrays were far apart, they can be treated as two separate specimens (H1a and H1b or H7a and H7b), with the same far field applied stain but different local fiber spacing.

Composite creep tests were performed at 40°C, 50°C, and 80°C. A constant uniform stress was applied to the samples using custom-built jigs and a strain gage was directly attached to the sample surface to monitor the macro-strain $\varepsilon^*(\mathcal{T})$. The applied load was increased gradually until a break was observed in a fiber and then held constant. The sample was held in a modified tensile jig with a custom-built heater in the middle, which was connected to a temperature control device (not shown in Fig. 4). Temperature was monitored by a thermocouple

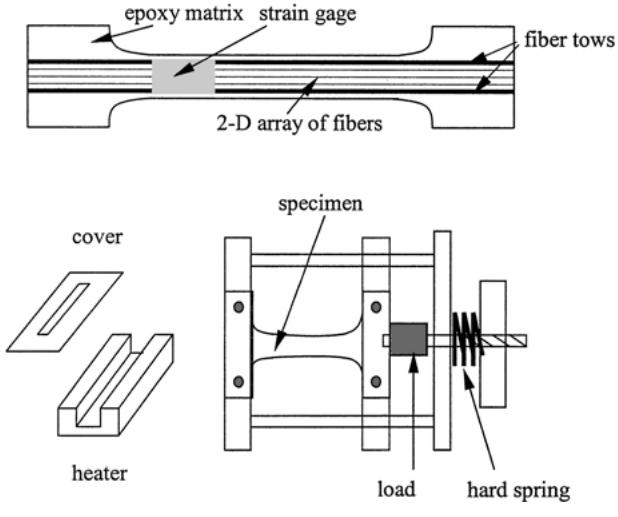


*Figure 4* Geometry of the composite specimens and the custom-built tensile jig with an attachable heater, connected to a temperature control device (not shown).

TABLE I Summary of the model composite samples tested at elevated temperatures

| Sample no. | Temperature (°C) | Fiber spacing $w$ ($\mu$m) | Far field fiber strain (%) | Matrix strain (%) |
|---|---|---|---|---|
| H1a | 40°C | 4 | 0.77–0.9 | 1.4–1.5 |
| H1b | 40°C | 30 | 0.77–0.9 | 1.4–1.5 |
| H2 | 50°C | >200 | 1.0–1.1 | 1.1–1.2 |
| H3 | 50°C | >200 | 0.8–0.85 | 1–1.05 |
| H4 | 50°C | 0–2 | 0.7–0.8 | 0.9–1.1 |
| H5 | 80°C | 0–1 | 0.65–0.7 | N/A |
| H6 | 80°C | 320 | 0.8–1.0 | N/A |
| H7a | 80°C | 0–1 | 0.25–0.3 | N/A |
| H7b | 80°C | 28 | 0.4–0.5 | N/A |

in the gage length of the composite sample. With a metal cover on top of the heater, the temperature variation was within ±1°C for tests at 40°C and 50°C, and within ±3°C for tests at 80°C. A small window in the middle of the cover allowed for Raman measurements on the fibers within the composite sample.

A Renishaw Ramanscope System 2000 connected to a 514 nm Argon ion laser was used to record the Raman spectra of the fiber during the creep tests, with a spatial resolution of approximately ±1 $\mu$m. Raman spectra were recorded along the fibers at periodic time intervals. The time required to record a single measurement was 20 seconds. Approximately 60 data points were collected to obtain a profile along a single fiber. Therefore the time required for one fiber profile was approximately 20–30 minutes and the time at the start of each acquisition period is associated with the time of each fiber profile. The *in situ* fiber strain distributions were determined from the Raman spectra of the Toray M40B fiber, which has a very well defined Raman peak around 2700 cm$^{-1}$. This peak shifts linearly to lower values as the fiber tensile strain increases. The slope of this linear relationship is referred to as the Raman frequency gauge factor (RFGF) [13]. For the graphite fiber in this work, RFGF is 25.35 ± 2 cm$^{-1}$/%. The axial strain $\varepsilon(x)$ at any point $x$ along a high performance fiber can be determined according to:

$$\varepsilon(x) = (v(x) - v_0)/\text{RFGF}, \quad \text{at a given measurement time} \tag{9}$$

where $v(x)$ and $v_0$ are the peak positions at point $x$ and at zero strain respectively.

### 3.2. Creep tests of the bulk epoxy matrix

The parameters in $J(\mathcal{T})$, Equations 1 and 2, are functions of stress level (or strain rate) as well as temperature. Tensile creep tests were performed at room temperature on bulk epoxy matrix specimens at three different stress levels (10 MPa, 20 MPa, 30 MPa) and various temperatures ranging from room temperature (25°C) to 80°C. The epoxy specimens had the same dog-bone geometry as the composite. The time evolution of the matrix creep compliance was fit to the two power law functions, Equations 1 and 2, in order to obtain the matrix parameters required by the SFM.

Assuming the polymer is isotropic, the shear compliance was determined by the following relation from the measured tensile compliance $S(\mathcal{T})$,

$$J(\mathcal{T}) = 2S(\mathcal{T})\{1 + v(\mathcal{T})\} \tag{10}$$

where $v(\mathcal{T})$ is the Poisson's ratio, which is taken to be a constant and $v = 0.33$.

## 4. Results

### 4.1. Bulk matrix creep tests

Fig. 5 shows the increase of the matrix compliance with time at three different stress levels (10 MPa, 20 MPa, 30 MPa) and at different temperatures (from room temperature up to 80°C). Overall, matrix creep deformation is accelerated at higher stress and higher temperature.

A time-temperature-stress superposition (TTSS) method was used to describe the matrix creep compliance, with the reference curve at 20 MPa and room temperature. For each curve, the parameters $J_1$, $\mathcal{T}_C$, and $\alpha$ associated with the creep compliance law (1) were determined. We found that the characteristic time

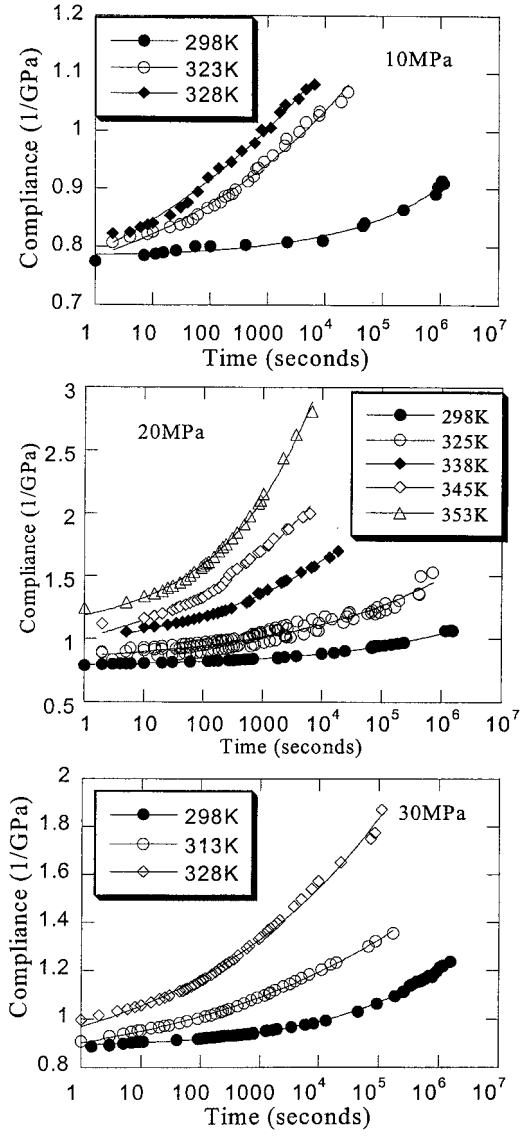


*Figure 5* Creep of the pure epoxy at different temperatures and different stresses.

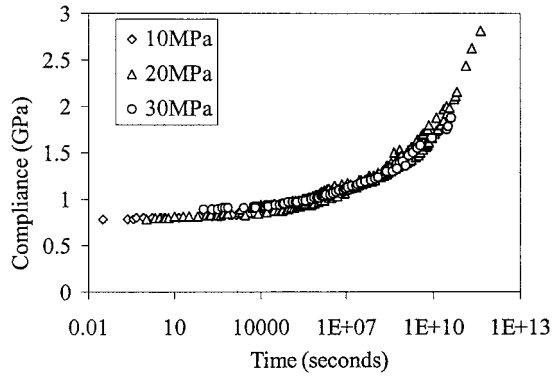


*Figure 6* Master curve for different temperatures and three different stress levels by time-temperature-stress superposition method.

$\mathcal{T}_C$ changed significantly with temperature and stress, whereas $J_1$ and $\alpha$ did not. Therefore for each curve in Fig. 5 determined its shift factor $a$, which is simply the horizontal distance required to coincide each curve with the reference curve in log time scale. Fig. 6 shows the master curve, with compliance parameters $J_1$, $\mathcal{T}_{C_m}$ and $\alpha$ determined to be 0.78 1/GPa, 2.5E+9 seconds, 0.16, respectively, where $\mathcal{T}_{C_m}$ is the characterization time of the master curve. Therefore with this method, the temperature and stress effects of this epoxy can be packaged in one matrix material parameter, the characterization time $\mathcal{T}_C = \mathcal{T}^*_{C_m} 10^{-a}$ where $a$ was a linear function of temperature and stress.

The power law parameters at 20 MPa were used in the model calculations, since the applied stress was ~20 MPa for the model composites. Both the matrix creep parameters determined from individual creep profiles and the calculated values from the TTSS method were used in the SFM predictions on the composite creep at different temperatures. It was found that the difference in the results was negligible which shows that the TTSS method is valid for the epoxy creep in the temperature and stress ranges in this work. Therefore the calculated TTSS values were used as the time constant in Equation 1 for all temperatures and stress levels.

### 4.2. Creep of the model composites

Among the composite regions analyzed, the fiber spacing $w$ varied from 1 $\mu$m to 320 $\mu$m (See Table I). In our previous work [8], it was observed that fiber spacing could affect the fiber strain profiles significantly by favoring debonding at relatively large $w$, and matrix yielding at small $w$. In the present work, very little or no slip was detected and matrix yielding dominated in all composite specimens at elevated temperature. Consistent with our findings in [8], Fig. 7 for sample H1 at 40°C shows that the effect of fiber spacing, from 4 $\mu$m to 30 $\mu$m was smaller than the scatter in the Raman data. Therefore, the effect of fiber spacing is ignored in the remaining comparisons.

The shape of the predicted strain profile depends on two factors: $\tau_c$, the shear stress in the inelastic zone, and $\gamma_c$, the critical shear strain for the onset of inelasticity. As will be described in the following, $\tau_c$ (or to be more specific, $\tau_p$ for the yielded zone and $\tau_d$ for the debonded

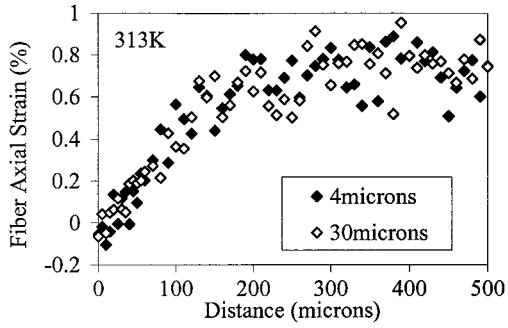


*Figure 7* Fiber strain distributions along the broken fibers for two different fiber spacings, $w = 4$ microns and $w = 30$ microns, in specimen H1 at 40°C.

zone) was determined by fitting the strain data in the linear zone to Equation 3. With $\tau_c$ known, $\gamma_c$ can be determined by comparing the predicted strain profile to the measured strain data.

As the matrix compliance changes with temperature, the fiber strain profiles along a broken fiber also change accordingly, as shown in Fig. 8 for two specimens, H1a (40°C) and H5 (80°C). For these two specimens, the far field fiber strains were similar and we suspect matrix yielding in the inelastic zone. As the temperature increases, the slope of the linear region near the fiber break ($x = 0$) decreases, which indicates a smaller $\tau_p$ in the inelastic zone. At the same time, the scattering in the strain data increases with temperature.

The temperature dependence of $\tau_p$ is more clearly shown in Fig. 9 for all specimens, where $\tau_p$ decreased with temperature, with the standard deviation as the error bars. This change can be well described empirically

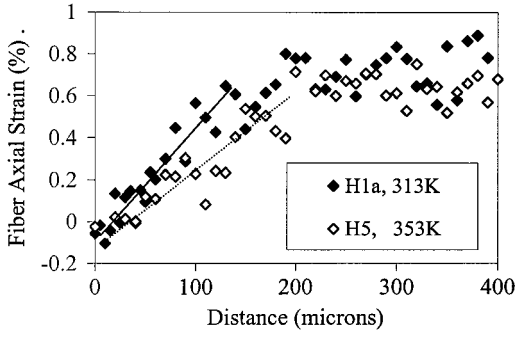


*Figure 8* Fiber strain distributions along a broken fiber at two different temperatures, 40°C and 80°C, with matrix yielding near the fiber break.

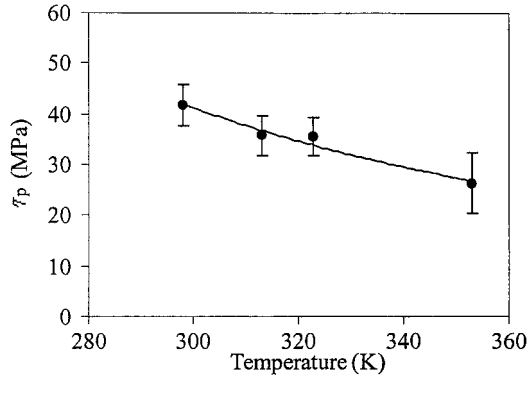


*Figure 9* Interfacial shear stress $\tau_p$ as a function of testing temperature.

$\tau_{p^*}$ with a simple power law function,

$$\tau_{p^*}(T) = A(T/T_g)^B = A(T/383\ \mathrm{K})^B \qquad (11)$$

where $A$ and $B$ are empirical parameters determined to be 22, and $-2.5$, respectively from data fitting and $T$ is temperature in K. The glass transition temperature for the epoxy matrix is 383 K.

Fig. 10 compares the SFM predictions at two times with the MRS data along a broken fiber in specimen H1 tested at 40°C. Taking into account the temperature dependence of $\tau_p$, the SFM predicts the strain distributions well, using the same criterion for inelasticity ($\gamma_c = 5\%$) as that used for room temperature [8]. Similar good agreement was observed for the fiber strain data at 50°C.

When the temperature was raised to 80°C, the same criterion ($\gamma_c = 5\%$) again works well for specimen H5, where matrix yielding dominated near the fiber break, as shown in Fig. 11a. In the inelastic zone in specimen

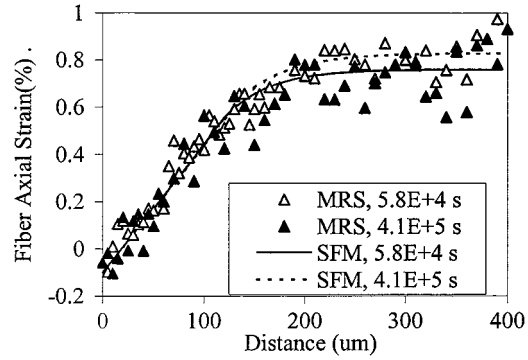


*Figure 10* Strain distributions along a broken fiber in sample H1 (40°C) with $w = 4$ $\mu$m at two different times, with the SFM predictions using $\gamma_c = 5\%$.

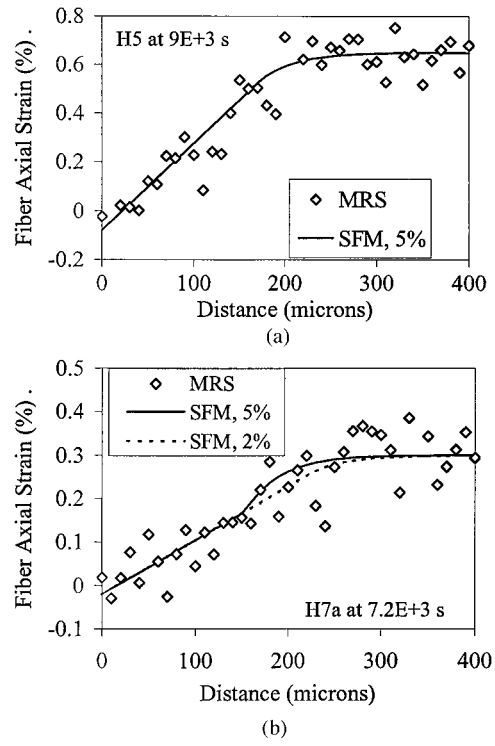


*Figure 11* Strain distributions along a broken fiber at 80°C with SFM predictions using different $\gamma_c$, 5% or 2% (a) sample H5, $\tau_c = 23$ MPa; (b) sample H7a, $\tau_c = 8$ MPa.

H5, $\tau_p = 23$ MPa. However, in specimen H7 (both H7a and b) the inter- face was poor and hence the frictional resistance was low, $\tau_d = 8$ MPa, a value that is characteristic of a debonded interface. The predicted inelastic length in H7 using $\gamma_c = 5\%$ is shorter than that indicated by the measured strain data. A better match was obtained using $\gamma_c = 2\%$, as seen in Fig. 11b. This suggests that the criterion for inelasticity could decrease gradually as temperature increases, although this change is not noticeable from model/data comparisons at 40°C and 50°C. Therefore $\gamma_c = 5\%$ is used for the model predictions in Figs 12 and 13. More experimental data are needed to analyze the temperature dependence of the critical shear strain.

This model and results of our study are used to forecast the influence of inelastic zone type (debonding vs. plasticity) on the growth of inelastic zones over long times and elevated temperatures. Fig. 12 shows the SFM predictions $l(t)$ when the applied strain $\varepsilon^* = 0.7\%$ and $w = 1$ $\mu$m and at three different testing temperatures (25°C, 40°C, 80°C) and under different interfacial conditions. In all specimens in Fig. 12a, matrix yielding dominates and $\tau_{p^*}(T)$ at each temperature is calculated from the power law function in Fig. 9. The growth rate of the plastic zone length $l_p$ increases with temperature. However, the change is still not very significant during a time interval from 1E+3 seconds to 1E+8 seconds, which corresponds to more than 1000 days. As seen in Fig. 12a, $l_p$ increases from 133 $\mu$m to 151 $\mu$m during this period even at 80°C, when the temperature is only 30°C below its glass transition temperature $T_g$. When interfacial debonding is the major mechanism near a fiber break, the inelastic length $l_d$ is longer than $l_p$ and grows at a higher rate, as shown in Fig. 12b. Since the temperature dependence of $\tau_d$ could not be characterized here, a constant $\tau_d$ (10 MPa) is assumed. In this case, $l_d$ increases from 360 $\mu$m to 410 $\mu$m from 1E+3 seconds to 1E+8 seconds at 80°C.

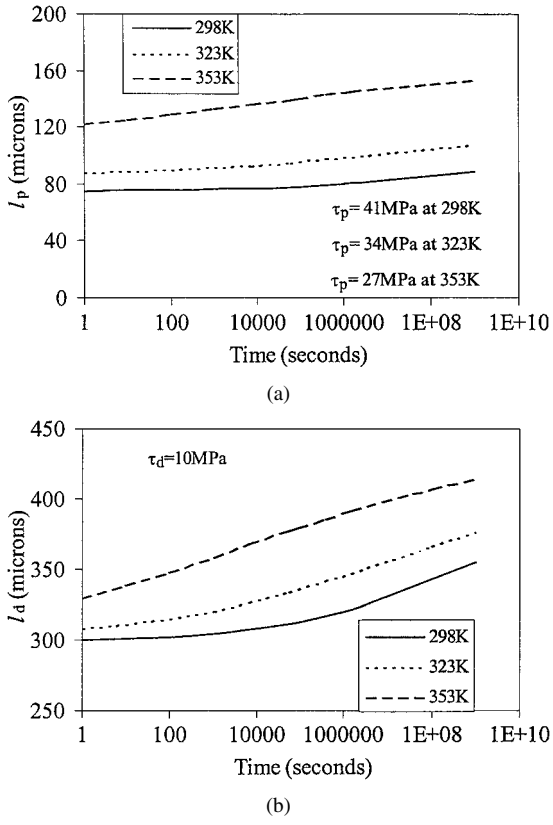


*Figure 12* Increase in the inelastic length $l_{in}$ at different temperatures with $w = 1$ $\mu$m and $\varepsilon^* = 0.7\%$ under different interfacial conditions (a) matrix yielding dominated, with $\tau_p$ calculated from the power law function in Fig. 6.2 (b) debonding dominated, with a constant $\tau_d = 10$ MPa.

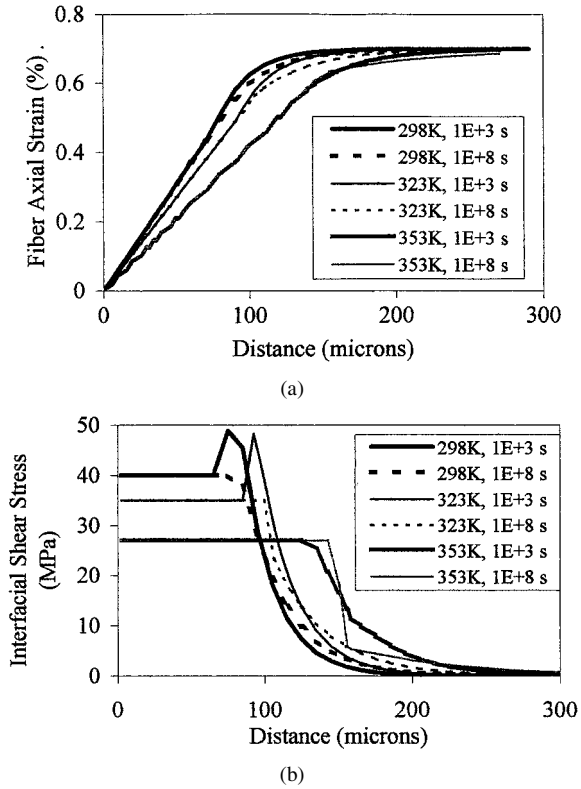


*Figure 13* SFM predictions for fiber axial strain and interfacial shear stress with $w = 1$ $\mu$m and $\varepsilon^* = 0.7\%$ under different temperatures at two different times when the interface near a fiber break is dominated by matrix yielding (a) fiber axial strain; (b) interfacial shear stress.

Fig. 13 shows the corresponding strain/stress distributions in the broken fiber at three temperatures each with different $\tau_p$ corresponding to Fig. 12a. Since there is little change in $\tau_p$ and $l_p$ with temperature, there is only small change in the fiber strain profile in the elastic zone. This indicates that the micromechanics around an isolated break is quite stable when matrix plasticity dominates near the fiber break. Although debonding and slip are also likely near a fiber break, the debonded zone is usually much larger than the yielded zone. For these model composites tested at elevated temperatures, the only exception is sample H7, where the interface behavior was dominated by debonding.

Although matrix yielding and interfacial slip are different mechanisms, they are all labeled as 'inelastic' in the constitutive law in Fig. 3, differing only in the value. We choose to use this simple elastic-inelastic law, instead of the more complex elastic-plastic-slip law [8], since only one clearly linear section of the measured fiber strain profile can be reasonably identified. Usually matrix yielding is assumed when the interfacial shear stress $\tau_c$ is in the range of matrix yielding strength. When $\tau_c$ is much below that range, interfacial slip is a more accurate description. Our MRS measurements suggest that the yield strength of the epoxy in this work is 40–50 MPa at room temperature and decreases to 20–30 MPa at 80°C. Such decreases in epoxy yield

strength with increase in temperature have been observed and reported elsewhere [11]. At a given applied strain $\varepsilon^*$, such decreases in $\tau_c$ with temperature will increase the inelastic length $l(t)$ emanating from the break according to the SFM predictions, (See Figs 11–13).

## 5. Discussions and conclusions

The strain/stress redistribution during creep at elevated temperature along broken fibers in multifiber composites was investigated by MRS and compared with the predictions from the SFM. Elevated temperatures changed the local creep response around fractures at a rate depending on the type of inelastic damage generated. In our composite system, local matrix inelasticity was favored over interfacial debonding and as a result, the time evolution of inelastic zones and stress transfer was relatively slow and virtually independent of local fiber volume fraction. These results were interpreted by a representative single fiber model, which accounted for the micromechanics of matrix plasticity, viscoelasticity and interfacial frictional slip.

The important material parameters used in the constitutive law for the matrix or interface (See Fig. 3) are $\tau_p$ or $\tau_d$, and $\gamma_c$, the resistant plastic or frictional shear stress respectively, and critical shear strain. Both $\tau_p$ and $\gamma_c$ are shown to be influenced by temperature. At a higher temperature, a smaller plastic shear stress $\tau_p$ leads to a longer inelastic length, which is usually comparable to the 'unloaded' length near a fiber break. The positive affected length (PAL) in the neighboring intact fiber is considered to be proportional to the 'unloaded' length in the broken fiber. Therefore, our results suggest that the PAL will increase with temperature. Since longer lengths of intact fibers will be exposed to stress concentration with increasing temperature and time, the failure probabilities in neighboring fibers will be increased as well.

The comparison of the SFM predictions with the MRS data in specimen H7 suggests that the critical shear strain $\gamma_c$ could be lower at a higher temperature. Miwa and Endo [12] presented the temperature dependence of shear yield strength and the Young's modulus of an epoxy resin, from which a decrease in shear yield strain could be inferred. Further investigation is needed to establish the relationship between $\gamma_c$ and temperature. The decrease in $\gamma_c$ will also increase the inelastic length and hence broaden the stress concentration in the neighboring fibers.

The SFM works well in predicting the time evolution of strain/stress along a broken fiber within multifiber composite specimens, varying widely in fiber volume fraction at elevated temperatures. In the model, the temperature dependence of $\tau_p$ is considered. At a specific temperature, $\tau_p$ is assumed to be constant, since little or small change was observed during testing period for an isolated break. If any change is found in $\tau_p$ for other composite systems or longer testing time, the change could be readily accommodated in this and our other micromechanical models.

The simple SFM captures the important features in the strain/stress evolutions at elevated temperature and provides guidance for future improvements in some multi-fiber composite models. Since the creep-rupture of the polymer composites is a complex process, microdamage development through fiber-fiber interactions should also be considered, which is possible only in a multi-fiber composite model.

## Acknowledgments

This work was supported by National Science Foundation (No. CMS-9800128) and a Directed Research and Development Project at Los Alamos National Laboratory (No. 2000043). The authors also appreciated the technical assistance from Mr. D. Van Steele and Mr. R. Dove at Rensselaer Polytechnic Institute.

## References

1. K. C. GRAMOLL, D. A. DILLARD and H. F. BRINSON, *Comp. Mater. Testing and Design* **9** (1990) 477.
2. J. H. GREENWOOD, *Composites* **9** (1975) 203.
3. C. GALIOTIS, R. J. YOUNG and D. N. BATCHELDER, *J. Mater. Sci. Lett.* **6**(2) (1983) 263.
4. T. MIYAKE, T. YAMAKAWA and N. OHNO, *J. Mater. Sci.* **33** (1998) 5177.
5. J. S. THOMSEN and R. PYRZ, *Compos. Sci. Technol.* **59** (1999) 1375.
6. *Idem.*, *ibid.* **60** (2000) 1791.
7. C. H. ZHOU, L. S. SCHADLER and I. J. BEYERLEIN, *Acta Materialia* **50** (2002) 365.
8. I. J. BEYERLEIN, C. H. ZHOU and L. S. SCHADLER, *Inter. J. Solid Struct.*, Accepted.
9. I. J. BEYERLEIN, S. L. PHOENIX and R. RAJ, *ibid.* **35** (1998) 3177.
10. I. J. BEYERLEIN, *Comp. Sci. Technol.* **60** (2000) 2309.
11. M. MIWA, A. TAKENO, T. YOKOI and A. WATANABE, *J. Mater. Sci.* **34** (1999) 5489.
12. M. MIWA and I. ENDO, *ibid.* **29** (1994) 1174.
13. N. MELANITIS and C. GALIOTIS, *ibid.* **28** (1990) 5081.

*Received 18 June*
*and accepted 30 October 2002*